Photochemical & Photobiological Sciences (2022) 21:1991–2000
https://doi.org/10.1007/s43630-022-00273-5

ORIGINAL PAPERS

Nitrogen-doped, proton-exchanged Dion-Jacobson layered niobate perovskites for photocatalytic hydrogen generation in solar light

Natalia Kulischow[1] · Mirco Ade[2] · Morten Weiss[2] · Roland Marschall[2]

Received: 28 March 2022 / Accepted: 13 July 2022 / Published online: 1 August 2022

Abstract

Wide band gap semiconductor niobate photocatalysts with Dion-Jacobson layered perovskite structure were nitrogen-doped via simple gas–solid reaction to extend their absorption into the visible light range. Nitrogen doping was performed using ammonia as precursor, resulting in decreased band gaps of doped $AB_2Nb_3O_{10}$ compounds (A = Cs, Rb, K; B = Ca, Sr) down to 2.5 eV. The resulting materials were investigated concerning their chemical and electronic structures. Nitrogen-doped $AB_2Nb_3O_{10}$ crystals showed a clear red shift in absorption. Photocatalytic performance tests for the doped materials evaluated the capability of H_2 production under simulated solar irradiation. The addition of carbonates to the gas–solid reaction turned out to be advantageous for the reduction of defects and the preservation of photocatalytic activity of nitrogen-doped layered niobates $AB_2Nb_3O_{10}$.

Graphical Abstract

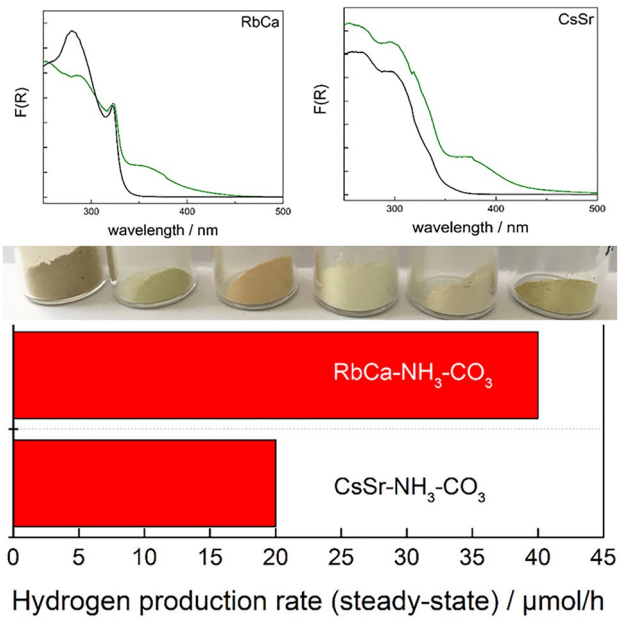

Keywords Ammonolysis · Layered perovskite · Nitrogen doping · Photocatalysis · Hydrogen generation

✉ Roland Marschall
Roland.marschall@uni-bayreuth.de

[1] Institute of Physical Chemistry, Justus-Liebig-University Giessen, 35392 Giessen, Germany

[2] Department of Chemistry, University of Bayreuth, 95447 Bayreuth, Germany

1 Introduction

Photocatalysis with semiconductors as light absorbers has been studied intensively because of the potential applications in clean energy and environmental remediation, for example in water splitting for storage of solar energy to chemical energy, [1] and photocatalytic degradation of pollutants in water and air [2]. In order to achieve efficient and sustainable solar energy conversion, the photocatalyst should have a small band gap (< 3 eV). Such visible light activity still remains a key challenge in the area of photocatalysis. Most of the active photocatalysts including many highly stable d^0 oxide semiconductor materials exhibit band gaps in the UV range, [3] such as TiO_2 (3.0 eV and 3.2 eV for rutile and anatase, respectively). This allows such photocatalysts to absorb solely UV light, which only accounts for around 5% of the total solar energy. Extending the band gap of photocatalysts into the wide visible light region seems a logical solution to this problem, since this would enable the photocatalyst to utilize the much larger portion of visible light energy.

Therefore, Asahi et al. introduced nitrogen doping in 2001 to reduce the band gap of oxide semiconductors [4]. Due to the insertion of N 2p orbitals, mid-gap states were introduced, effectively shifting the absorption of N-doped TiO_2 into the visible light range.

Wang et al. later showed that the crystal structure has an influence on the dopant distribution [5]. Treating layered titanates in ammonia gas, they achieved homogeneous nitrogen doping throughout the material due to the open crystal structure, enabling band-to-band visible light photon excitation by mixing of O 2p and N 2p orbitals forming a new valence band [6]. Following up on this, comparable examples of nitrogen-doped materials with layered or tunnel-like open crystal structure were reported to exhibit homogeneous nitrogen doping and visible light activity in photocatalysis [7–12].

Interestingly, very little examples of N-doped layered niobates have been reported [13, 14]. The reason might be that in many cases, Nb^{4+} and oxygen defects are formed leading to low photocatalytic activity [15], sometimes also referred to as Nb self-doping [16]. To reduce the amount of self-doping, mixing niobium oxides with carbonate salt was reported to reduce the extent of self-doping, leading to yellow N-doped $KCa_2Nb_3O_{10}$ [15].

Recently, we showed that proton exchange of $KCa_2Nb_3O_{10}$ can lead to a strong enhancement in photocatalytic activity for hydrogen evolution [17]. Here, we combine the latter two strategies, presenting nitrogen-doped proton-exchanged Dion-Jacobson layered niobate perovskites for solar hydrogen generation. We present two strategies to reduce defects formed upon ammonolysis, namely oxygen post-treatment and carbonate addition. The latter one-step preparation leads to lower amount of defects in the doped materials, and the highest photocatalytic activities among the nitrogen-doped layered niobate nanosheets studied.

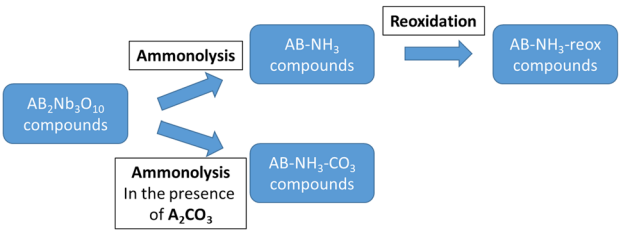

Scheme 1 Synthesis procedure for N-doped $AB_2Nb_3O_{10}$ layered perovskites

1.1 Experimental

All chemicals were of analytical grade and used as received. Ammonia gas (Praxair, 99.99%), Cs_2CO_3 (Alfa Aesar, 99.9%), K_2CO_3 (Grüssing, 99.0%), methanol (J. T. Baker, a. g.), Na_3RhCl_6 (Sigma-Aldrich, 99.9%), Rb_2CO_3 (Sigma-Aldrich, 99.8%), oxygen gas (Linde, 99.99%).

Bulk material $AB_2Nb_3O_{10}$ compounds (A = Cs, Rb, K; B = Ca, Sr) were prepared via the molten salt synthesis described previously [18]. The material will be denoted AB, according to their respective cations.

For the nitrogen doping with ammonia gas, a tube furnace equipped with a quartz tube was used. Software and mass flow controllers regulated the temperature and gas flow. 300 mg of the bulk material was placed in a ceramic boat and exposed to 75 mL/min NH_3 gas flow at 800 °C for 1 h, resulting in black powders. Samples will be denoted comparable to the untreated samples, AB-NH_3.

When treated under NH_3 gas flow and re-oxidized with oxygen (5 mL/min at 500 °C for 5 min), this resulted in light yellow and lemon green coloured powders. Samples will be denoted comparable to the untreated samples, AB-NH_3reox.

When bulk material was mixed with 20% excess of A_2CO_3 (A = Cs, Rb, K) before NH_3 gas treatment, the ammonolysis resulted in light yellow and lemon green coloured powders. Samples will be denoted comparable to the untreated samples, AB-NH_3-CO_3 Scheme 1 gives an overview on the synthesis procedure.

For photocatalysis, all of the nitrogen doped materials were proton exchanged through the method described previously [17].

X-ray diffraction patterns were measured on a PANalytical MPD diffractometer using Cu-Kα radiation ($\lambda = 0.1541$ nm) in the 2θ range from 5 to 55. The phase

purity was confirmed using the HighScore Plus software version 3.0e (3.0.5) and the ICSD database.

UV–vis was performed on a PerkinElmer Lambda 750 UV–vis–NIR spectrometer, using a Praying Mantis mirror construction from Harrick.

X-ray photoelectron spectroscopy (XPS) was measured with a VersaProbe III Scanning XPS Microprobe from Physical Electronics (III), with a monochromatic Al K_α source and a beam diameter of 100 µm. Survey spectra were measured with step size of 0.4 eV and a pass energy of 224 eV, high-resolution spectra were measured with a step size 0.1 eV and a pass energy of 26 eV; the time per step was 50 ms in both cases. Slow moving electrons and Ar ions were used for sample charge neutralisation. Sputter-cleaned beforehand was omitted to avoid surface reduction by preferential sputtering. Data were analysed with CasaXPS using Shirley backgrounds and Gaussian–Lorentzian (GL30) peak shapes. The C 1 s signal was set to 284.8 eV for charge correction. The Nb 3d signal was fitted using a constrained area ratio of 2:3 for the $3d_{3/2}$ and $3d_{5/2}$ doublet, a peak separation of 2.72 eV, [19] and equal FWHM for the peaks of the doublet.

The morphologies of the compounds were investigated by field emission scanning electron microscopy (FESEM, Zeiss LEO 1530). An acceleration voltage of 3 kV was used together with a working distance of 8 mm and an aperture set to 30 µm. The energy dispersive X-ray analysis EDX) were performed with the same device though an acceleration voltage of 20 kV and an aperture of 60 µm were applied.

Hydrogen production experiments were conducted in a 120 mL volume double-walled glass reactor with quartz top. To avoid any thermal catalytic effect, the reactor was cooled down to 20 °C using a double walled jacket, through which cooling water was circulated from a thermostat (Lauda). High purity argon was used as the carrier gas for the reaction products. The flow rate was set at 25 mL/min and controlled by Bronkhorst mass flow controller. The evolved hydrogen was detected using a Shimadzu GC-2014 gas chromatograph equipped with a thermal conductivity (TCD) detector and RESTEK Shin-Carbon ST 100/120 column. Gas separation was achieved isothermal at 35 °C, afterwards the column was heated to remove adsorbed water. In a typical experiment, 30 mg photocatalyst were dispersed in 108 mL H_2O and 12 mL MeOH. Prior to irradiation, the system was purged with argon at 100 mL/min to ensure complete air removal. 0.05 wt.−% Rh co-catalyst were in-situ photodeposited on the catalyst from Na_3RhCl_6 introduced in the system with a syringe through a reactor inlet rubber sealing. The solution was stirred constantly. As light source, a 150 W Xe solar light simulator (Newport Sol 1A) was used.

2 Results and discussion

X-ray powder diffraction patterns of the pristine $AB_2Nb_3O_{10}$ compounds are presented in Fig. 1. All samples show high crystallinity and reflections characteristic for the respective single-phase Dion-Jacobson layered perovskites [18]. The XRD analysis shows that the nitrogen doping with ammonia gas has no influence on the material structure, hardly any changes can be observed in the XRD patterns after ammonolysis. This confirms that no transformation to oxynitrides has taken place.

SEM images after ammonolysis (Fig. 2) show sheet-like material with small and larger crystallites, as known from the bulk material, even after the ammonia treatment at 800 °C. For comparable images of the bulk materials, we refer to our earlier work [18].

Figure 3 shows absorption spectra for $AB_2Nb_3O_{10}$ compounds and of nitrogen-doped counterparts, respectively. The amount of nitrogen doping from XPS ranges from 0.1 at.−% (KCa) to 6 at.−% (RbSr) under the same reaction conditions. It is clear that nitrogen doping results in a change of the absorption from band gaps of around 340–350 nm to a broad visible light absorption. Utilizing visible light for photocatalytic hydrogen generation is a key challenge, and visible light absorption of a material is a prerequisite for visible light activity. In contrast to the pristine $AB_2Nb_3O_{10}$ compounds, the large red-shift by N-doping is in most of the cases very pronounced and comparable to other nitrogen-doped layered titanates or tantalates [5, 8].

However, as the increased baseline suggests, strong amounts of defects were generated upon ammonia treatment. All samples exhibited grey to black colour after ammonolysis (Figure S1) indicating niobium and oxygen defects [20].

To reduce the amount of defects, especially on the surface to reduce the extent of surface recombination, nitrogen-doped samples were treated additionally for a short re-oxidation process in pure oxygen. As a result, green-yellowish samples were gained (Figure S2).

The respective XRD patterns show no structural changes, as expected, upon this treatment (Fig. 1). The morphology of the materials also hardly changes, as can be seen in the SEM images (Figure S3), and the elemental distribution of all elements is highly homogeneous. (Figure S4).

Interestingly, the absorption spectra show distinct changes. As can also be seen in Fig. 3, the baseline of the absorption spectra is recovered to nearly zero baseline, indicating healed surface defects upon treatment in oxygen.

Unfortunately, the reaction seems to go in line with reduced visible light absorption, since the absorption shift

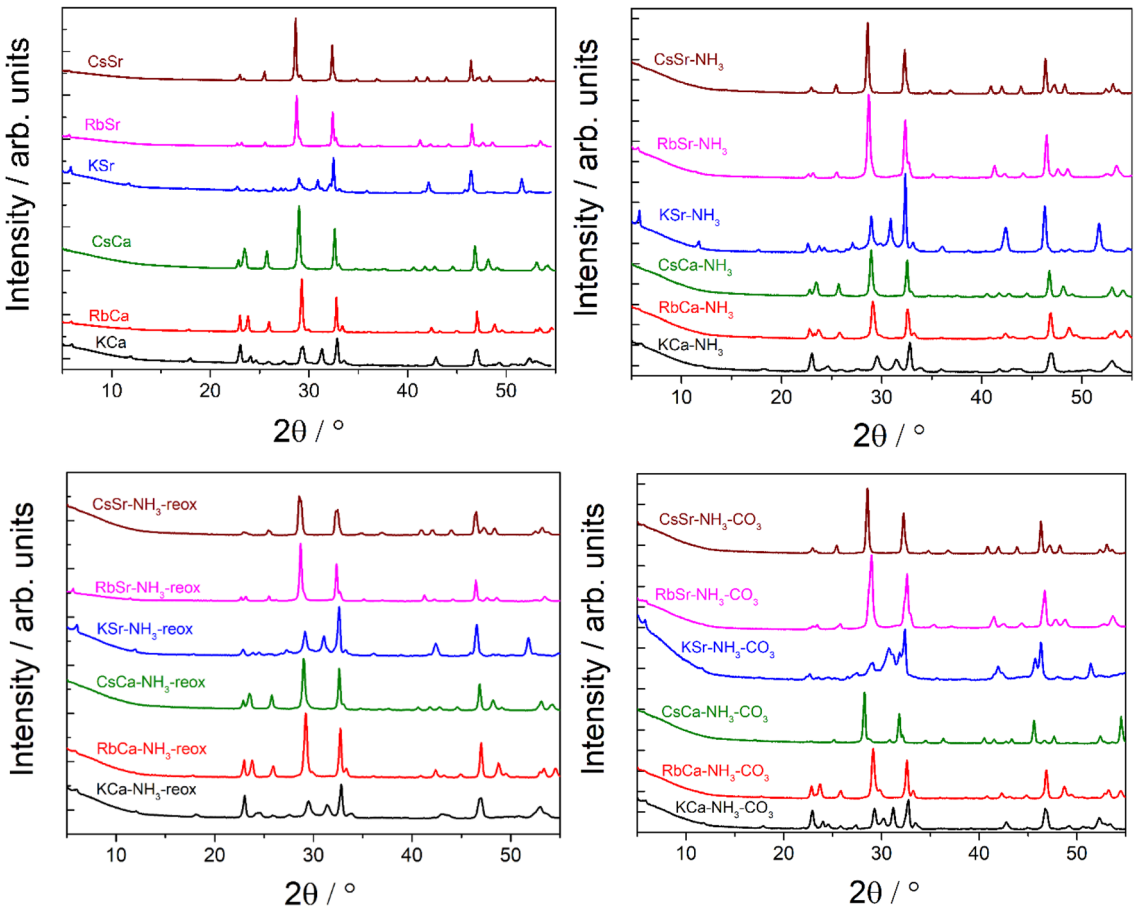

Fig. 1 XRD patterns of pure (top left) and N-doped layered perovskites. The respective sample names indicate the doping pathway from Scheme 1

into the visible light region is less pronounced, in some cases only resulting in absorption shoulders left. This indicates that the absorption shifts observed after ammonia treatment are a superposition of extended light absorption due to mixing of O 2p and N 2p orbitals, and due to defect formation.

The black materials, before proton exchange, are known in literature to contain too many oxygen defects in the crystal structure, and exhibit catalytic activity for hydrogen production only under UV irradiation [15]. Using a solar simulator (AM1.5G), we could confirm that none of the doped bulk materials, prior to H-exchange, show any activity for hydrogen evolution under solar simulation (not shown). Only after proton exchange, the doped compounds show activity under the desired conditions.

The hydrogen production experiments in aqueous suspension with methanol as a sacrificial agent (electron donor) of the proton-exchanged, nitrogen-doped dark compounds reveal that hydrogen can be generated after Rh decoration (Fig. 4). The experiments were performed under simulated sunlight (AM1.5G, 1000 W m^{-2}) containing small amount of UV light (< 5%), the hydrogen evolution rate trajectories are given in the Supporting Information (Figure S5). As can be seen, for the most active compounds, the evolution rates are very stable over time. The highest activity can be observed for $HCa_2Nb_3O_{10-x}N_x$ and $HSr_2Nb_3O_{10-x}N_x$, the latter one also being the most active material as proton-exchanged undoped oxide under UV light [17]. Without proton exchange, no activity was observed, as expected [15]. As for the undoped materials, due to their band gap no photocatalytic activity under sun simulation can be observed (not shown).

The re-oxidated materials show, in some cases, considerably higher H_2 production activity (the development of hydrogen evolution rates over time shown in Figure S6). The best activity was observed for NH_3-treated, re-oxidized and proton-exchanged $RbCa_2Nb_3O_{10-x}N_x$ with up to 32 µmol/h steady-state hydrogen evolution rate. The short re-oxidation process for the black-coloured layered perovskite sample resulted in a nearly 300% increase in photocatalytic efficiency compared to its black-coloured counterpart under similar reaction conditions.

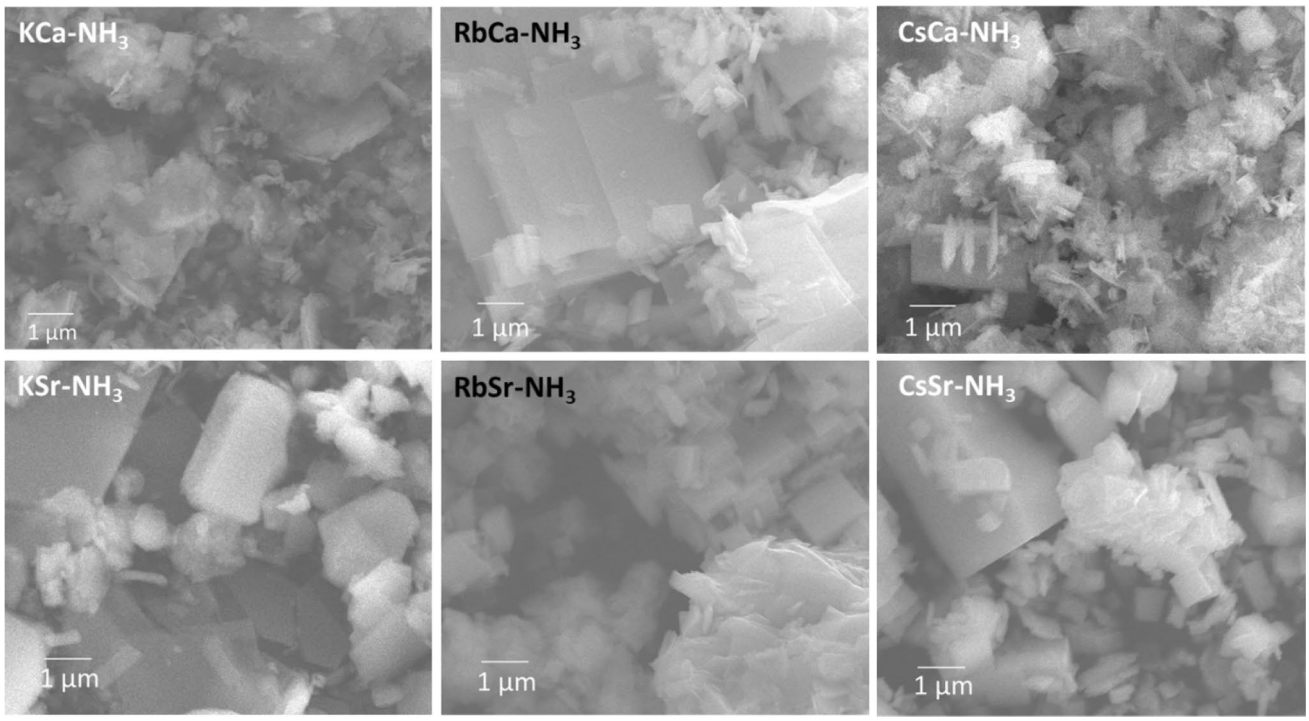

Fig. 2 SEM images of ammonia-treated AB-NH_3 layered perovskites for 1 h at 800 °C

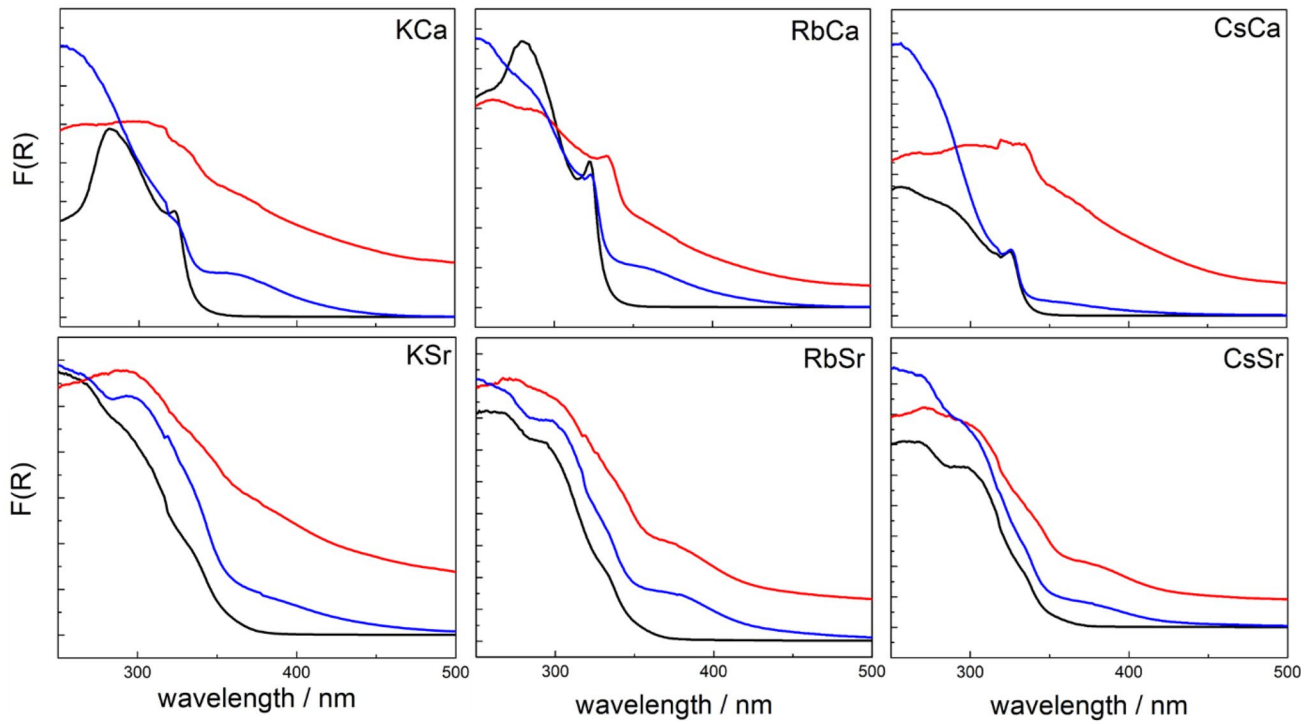

Fig. 3 Absorption spectra of bulk $AB_2Nb_3O_{10}$ compounds (black) compared to the respective spectra after nitrogen doping (red) of $AB_2Nb_3O_{10}$ compounds and after nitrogen doping and re-oxidation (AB-NH_3-reox, blue)

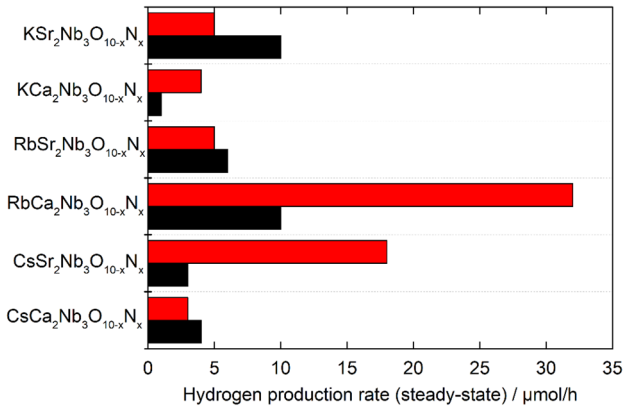

Fig. 4 H_2 production rate comparison of proton-exchanged, nitrogen-doped layered perovskites decorated with 0.05 wt.-% Rh co-catalyst under solar irradiation (black); in red are the activities after re-oxidation in oxygen gas. Conditions: 30 mg photocatalyst in 120 mL 10% methanol solution or 100 mg in 200 mL 10% methanol solution (back-calculated to 30 mg for comparison), 150 W solar simulator

In order to explain this behaviour, XPS was performed on $RbCa_2Nb_3O_{10}$ to unveil the defects present in the layered perovskite samples (Fig. 5). High-resolution XP spectra of Nb 3d region are very complex and reveal three different signals, which are split in $3d_{3/2}$ and $3d_{5/2}$, respectively. The most prominent one ranges from 206.1 eV to 206.5 eV (all values for $3d_{5/2}$); we ascribe this $3d_{5/2}$ signal to oxidic Nb(V) species of mixed oxides. It is commonly observed that binding energies of ternary, or quaternary metal oxides are slightly lower in binding energies compared to the simple binary oxides [19]. Reported binding energy values for ternary Nb oxides are only slightly higher than the energies observed herein [19, 21]. Thus, we assign the second signal in the high-resolution Nb spectra centred around 207.0 eV more likely to be due to Nb(IV) defects, which fits close to reported values for $CsNbTeO_6$ [22]. Additionally, there is a third, minor signal in the range from 204.7 eV to 204.9 eV, which is similar to binding energies reported for NbON [23–25].

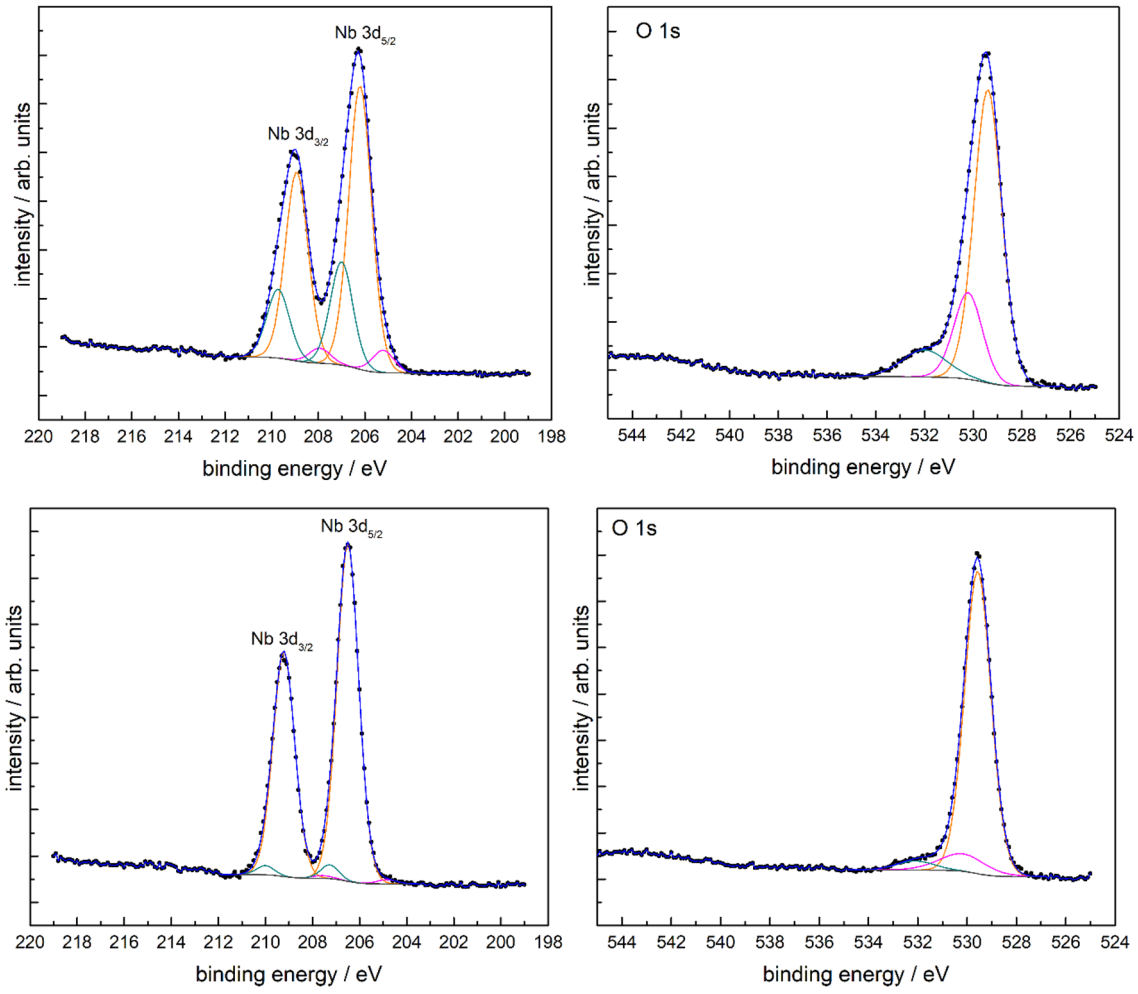

Fig. 5 High-resolution XP spectra of $RbCa_2Nb_3O_{10-x}N_x$ of niobium and oxygen regions, respectively. Upper row: after ammonolysis, lower row: after re-oxidation

The O1s spectra also show three different signals: the most intense one is located at 529.3 eV-529.6 eV and can be attributed to lattice oxygen, this value is slightly lower than reported for Nb_2O_5 [23, 26]. The second peak (530.2 eV-530.4 eV) can be ascribed to defective oxygen—that is oxygen located near defects—which is commonly observed for metal oxides. The low intensity of the defective O1s peak confirms the Nb peak assignment, resulting in less Nb defects than oxidic Nb(V) oxide species. The third peak in the O1s spectrum can be assigned to carbon–oxygen species belonging to adventitious carbon.

Comparing the spectra before and after re-oxidation, two details can be concluded. First, the ammonia treatment does generate oxygen and niobium lattice defects. However, both are getting reduced in number by the re-oxidation process, explaining the lowered baseline in the absorption spectra. However, on the other hand the intensity for the NbON assignment is also reduced, indicating the release of nitrogen from the lattice. From survey scans, the amounts of nitrogen are 3.2 and 1.8 at.−%, respectively.

In order to perform nitrogen doping but reducing the defect formation in one step, addition of alkali metal carbonates to the ammonolysis step was suggested in literature for $KCa_2Nb_3O_{10}$ [15]. Here, we adapt this approach for all our Dion-Jacobson layered perovskite niobates.

As can be seen in Fig. 1, the addition of carbonates to the ammonolysis has in most cases no influence on the crystal structure of the materials, too. The exceptions are $CsCa_2Nb_3O_{10}$ and $KSr_2Nb_3O_{10}$. The ammonia treatment in the presence of their carbonates leads to structural changes and a different catalyst altogether.

Interestingly, however, the absorption spectra indicate much less defects generated upon carbonate additions. Figure 6 shows the absorption spectra after ammonolysis in the presence of carbonates. They appear very similar to the absorption spectra given in Fig. 3 for the re-oxidised materials, as can be seen also in the photographs of the samples (Figure S7) having yellowish colors rather than black-grey. Only $CsCa_2Nb_3O_{10}$ and $KCa_2Nb_3O_{10}$ appear very different. Since $CsCa_2Nb_3O_{10}$ also exhibited structural changes upon ammonolysis, as observed in XRD patterns, these spectra cannot be compared. In the case of $KCa_2Nb_3O_{10}$, the shift in absorption into the visible light region is very prominent and far more pronounced compared to ammonolysis without carbonate and re-oxidation, however this cannot be converted into photocatalytic activity. SEM images of the respective samples show clear changes in the morphologies of $CsCa_2Nb_3O_{10}$ and $KCa_2Nb_3O_{10}$ in line with the XRD observations, besides no distinct morphology changes upon ammonolysis in the presence of carbonates (Figure S8) are observed for the other four materials.

Comparing the high resolution XP spectra after ammonolysis in the presence of carbonates for $RbCa_2Nb_3O_{10}$ (Fig. 7) with XPS data shown in Fig. 5, it can clearly be seen

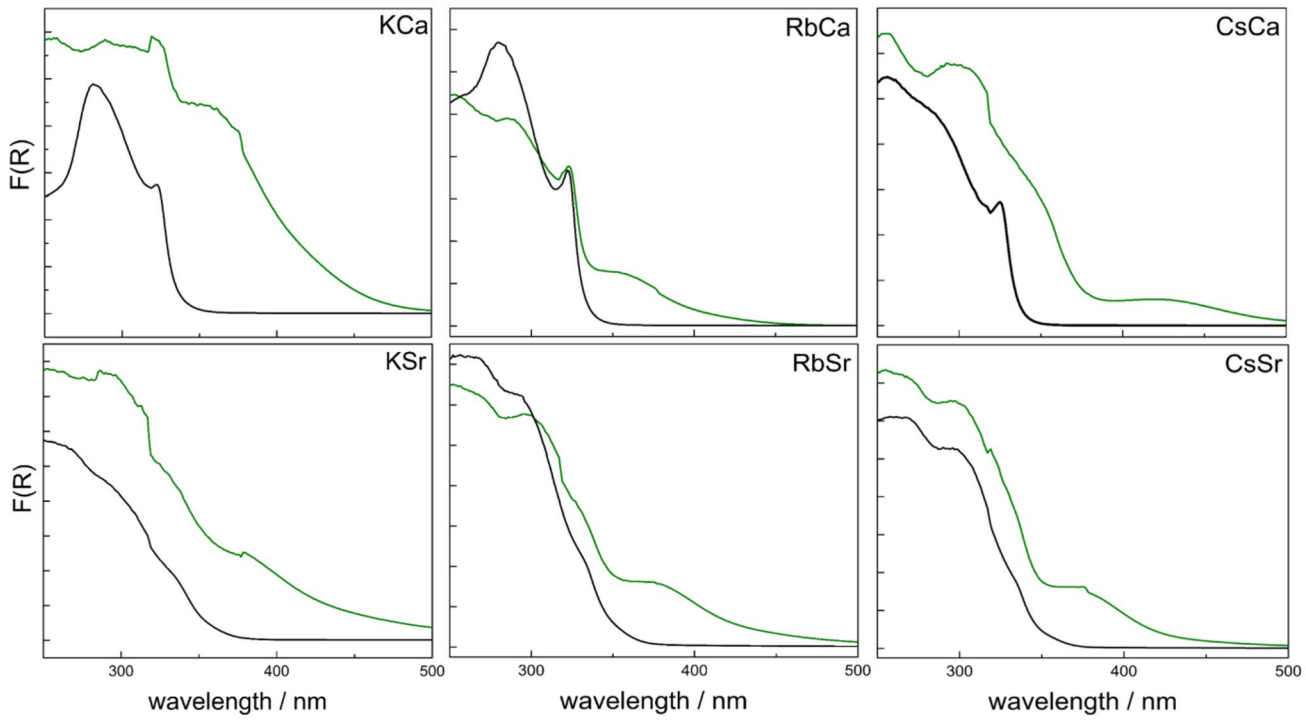

Fig. 6 Absorption spectra of bulk $AB_2Nb_3O_{10}$ (black) compared to the respective spectra after nitrogen doping via ammonolysis in the presence of A_2CO_3 (AB-NH_3-CO_3, green)

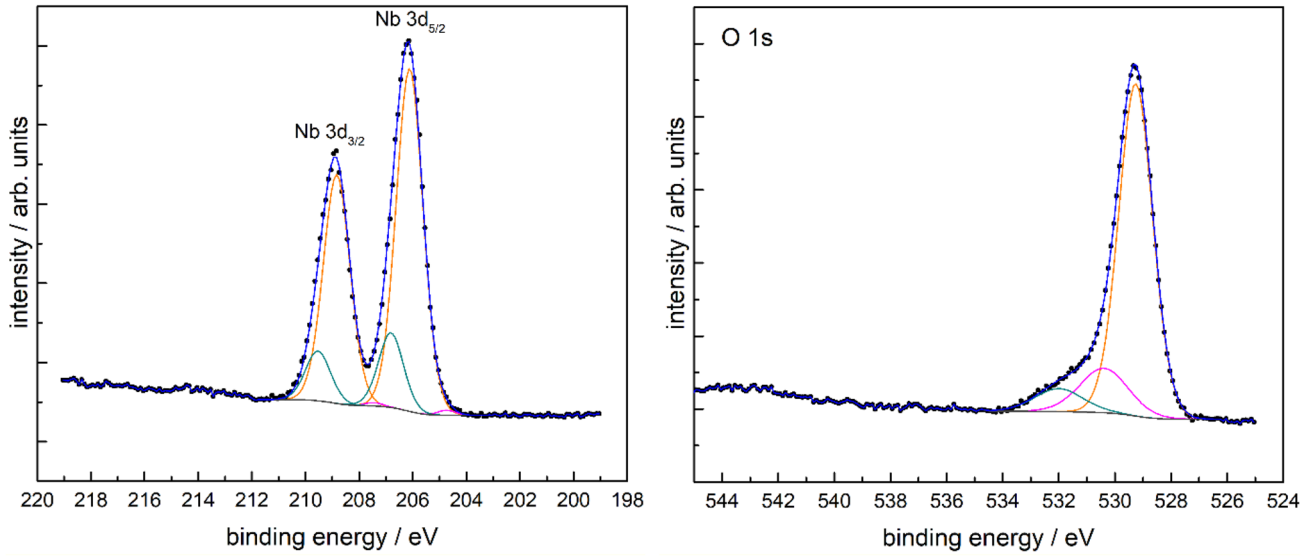

Fig. 7 High-resolution XP spectra of $RbCa_2Nb_3O_{10-x}N_x$ of niobium and oxygen regions, respectively, after ammonolysis in the presence of carbonates

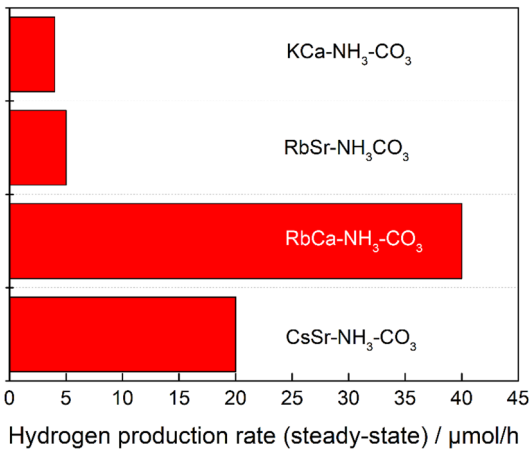

Fig. 8 H_2 production rate comparison of proton-exchanged, nitrogen-doped layered perovskites decorated with 0.05 wt.-% Rh co-catalyst under solar irradiation. Conditions: 30 mg photocatalyst in 120 mL 10% methanol solution, 150 W solar simulator

that the one step approach leads to lower amounts of lattice defects compared to sole ammonia treatment, hence the yellow colour. Moreover, nevertheless, the amount of NbON species is also lower, thus a trade-off between defect generation and nitrogen incorporation for the band gap reduction has to be considered.

The hydrogen production experiments in aqueous suspension with methanol as a sacrificial agent (electron donor) of the H-exchanged, N-doped (in the presence of carbonate) compounds reveal that hydrogen can be generated after proton exchange and Rh decoration (Fig. 8). The experiments were performed under simulated sunlight (AM1.5G) again. The hydrogen evolution rate trajectories are shown in Figure S9. The highest activity can be observed again for $HCa_2Nb_3O_{10-x}N_x$ derived from $RbCa_2Nb_3O_{10-x}N_x$, comparable to a sample after re-oxidation. Nevertheless, the activity is even higher now, with up to 40 µmol/h steady-state hydrogen production rate under solar light illumination. This value is 100% higher than for the second best material, $HSr_2Nb_3O_{10-x}N_x$ derived from $CsSr_2Nb_3O_{10-x}N_x$, and even higher than the best hydrogen production rates in Fig. 4.

Therefore, ammonolysis in the presence of A-cation carbonates can be considered a viable strategy for complex niobates to improve visible light absorption by nitrogen doping with reduced defect formation in one step, additionally preserving photocatalytic activity for hydrogen generation under sunlight illumination.

3 Conclusion

Defects generated upon ammonolysis of layered niobates $AB_2Nb_3O_{10}$ (A = Cs, Rb, K; B = Ca, Sr) can be reduced by two strategies, either subsequent re-oxidation with oxygen gas for several minutes, or by addition of A-cation carbonates to the pristine oxides during ammonolysis. Both pathways lead to band gap reductions into the visible light region for all six investigated layered niobates, and photocatalytic hydrogen generation upon sunlight illumination. The pathway using carbonates however leads to slightly higher activities, while at the same time enables a one-step preparation

route for several layered niobates to get nitrogen-doped layered niobate nanosheets for sunlight hydrogen generation.

Supplementary Information The online version contains supplementary material available at https://doi.org/10.1007/s43630-022-00273-5.

Acknowledgements We acknowledge financial support by the BMBF (Bundesministerium für Bildung und Forschung), research project DuaSol (03SF0482D). R. M. gratefully acknowledges funding in the Emmy-Noether program (MA 5392/3-1) of the German Research Foundation DFG. We thank the Bavarian Polymer Institute (BPI) (University of Bayreuth) Keylab "Device Engineering" for use of the XPS and the Keylab "Electron and Optical Microscopy" for use of SEM and EDX.

Funding Open Access funding enabled and organized by Projekt DEAL.

Declarations

Conflict of interest The authors declare no conflict of interest.

References

1. Marschall, R. (2021). 50 years of materials research for photocatalytic water splitting. *European Journal of Inorganic Chemistry, 2021*, 2435–2441.
2. Hoffmann, M. R., Martin, S. T., Choi, W. Y., & Bahnemann, D. W. (1995). Environmental applications of semiconductor photocatalysis. *Chemical Reviews, 95*, 69–96.
3. Kudo, A., & Miseki, Y. (2009). Heterogeneous photocatalyst materials for water splitting. *Chemical Society Reviews, 38*, 253–278.
4. Asahi, R., Morikawa, T., Ohwaki, T., Aoki, K., & Taga, Y. (2001). Visible-light photocatalysis in nitrogen-doped titanium oxides. *Science, 293*, 269–271.
5. Liu, G., Wang, L., Sun, C., Yan, X., Wang, X., Chen, Z., Smith, S. C., Cheng, H.-M., & Lu, G. Q. (2009). Band-to-band visible-light photon excitation and photoactivity induced by homogeneous nitrogen doping in layered titanates. *Chemistry of Materials, 21*, 1266–1274.
6. Liu, G., Wang, L., Sun, C., Chen, Z., Yan, X., Cheng, L., Cheng, H. M., & Lu, G. Q. M. (2009). Nitrogen-doped titania nanosheets towards visible light response. *Chemical Communications, 11*, 1383–1385.
7. Mukherji, A., Marschall, R., Tanksale, A., Sun, C., Smith, S. C., Lu, G. Q., & Wang, L. (2011). N-Doped CsTaWO6 as a new photocatalyst for hydrogen production from water splitting under solar irradiation. *Advanced Functional Materials, 21*, 126–132.
8. Mukherji, A., Seger, B., Lu, G. Q. M., & Wang, L. (2011). Nitrogen doped $Sr_2Ta_2O_7$ coupled with graphene sheets as photocatalysts for increased photocatalytic hydrogen production. *ACS Nano, 5*, 3483–3492.
9. Chen, S., Qi, Y., Liu, G., Yang, J., Zhang, F., & Li, C. (2014). A wide visible-light-responsive tunneled MgTa2O6-xNx photocatalyst for water oxidation and reduction. *Chemical Communications, 50*, 14415–14417.
10. Cui, J., Liu, T., Qi, Y., Zhao, D., Jia, M., Liu, G., Zhang, F., & Li, C. (2017). A wide visible light driven complex perovskite Ba(Mg1/3Ta2/3)O3-: XNy photocatalyst for water oxidation and reduction. *Journal of Materials Chemistry A, 5*, 18870–18877.
11. Adhikari, S. P., Hood, Z. D., Chen, V. W., More, K. L., Senevirathne, K., & Lachgar, A. (2018). Visible-light-active g-C3N4/N-doped Sr2Nb2O7 heterojunctions as photocatalysts for the hydrogen evolution reaction. *Sustainable Energy & Fuels, 2*, 2507–2515.
12. Marschall, R., & Wang, L. (2014). Non-metal doping of transition metal oxides for visible-light photocatalysis. *Catalysis Today, 225*, 111–135.
13. Matsumoto, Y., Koinuma, M., Iwanaga, Y., Sato, T., & Ida, S. (2009). N Doping of Oxide Nanosheets. *Journal of the American Chemical Society, 131*, 6644–6645.
14. Maeda, K., Tokunaga, Y., Hibino, K., Fujii, K., Nakaki, H., Uchiyama, T., Eguchi, M., Lu, D., Ida, S., Uchimoto, Y., & Yashima, M. (2018). New precursor route using a compositionally flexible layered oxide and nanosheets for improved nitrogen doping and photocatalytic activity. *ACS Applied Energy Materials, 1*, 1734–1741.
15. Zhou, Y., Wen, T., Guo, Y., Yang, B., & Wang, Y. (2016). Controllable doping of nitrogen and tetravalent niobium affords yellow and black calcium niobate nanosheets for enhanced photocatalytic hydrogen evolution. *RSC Advances, 6*, 64930–64936.
16. Zhou, Y., Wen, T., Kong, W., Yang, B., & Wang, Y. (2017). The impact of nitrogen doping and reduced-niobium self-doping on the photocatalytic activity of ultra-thin Nb3O8- nanosheets. *Dalt. Trans., 46*, 13854–13861.
17. Ladasiu, C., Kulischow, N., & Marschall, R. (2022). Tuning the photocatalytic activity of layered perovskite niobates by controlled ion exchange and hydration. *Catalysis Science & Technology, 12*, 1450–1457.
18. Kulischow, N., Ladasiu, C., & Marschall, R. (2017). Layered dion-jacobson type niobium oxides for photocatalytic hydrogen production prepared via molten salt synthesis. *Catalysis Today, 287*, 65–69.
19. J. F. Moulder, W. F. Stickle, P. E. Sobol and K. D. Bomben, Handbook of x-ray photoelectron spectroscopy, physical electronics. Eden Prairie. 1995.
20. Chen, X., Liu, L., Yu, P. Y., & Mao, S. S. (2011). Increasing solar absorption for photocatalysis with black hydrogenated titanium dioxide nanocrystals. *Science, 331*, 746–750.
21. Bahl, M. K. (1975). ESCA studies of some niobium compounds. *Journal of Physics and Chemistry of Solids, 36*, 485–491.
22. Weiss, M., Wirth, B., & Marschall, R. (2020). Photoinduced Defect and Surface Chemistry of Niobium Tellurium Oxides ANbTeO 6 (A = K, Rb, Cs) with Defect-Pyrochlore Structure. *Inorganic Chemistry, 59*, 8387–8395.
23. Havey, K. S., Zabinski, J. S., & Walck, S. D. (1997). The chemistry, structure, and resulting wear properties of magnetron-sputtered NbN thin films. *Thin Solid Films, 303*, 238–245.
24. Darlinski, A., & Halbritter, J. (1987). On the identification of interface oxides and interface serration by ARXPS. *Fresenius' Zeitschrift für Anal. Chemie, 329*, 266–271.
25. Darlinski, A., & Halbritter, J. (1987). Angle-resolved XPS studies of oxides at NbN, NbC, and Nb surfaces. *Surface and Interface Analysis, 10*, 223–237.

26. Yang, Z., Lu, X., Tan, W., Zhao, J., Yang, D., Yang, Y., He, Y., & Zhou, K. (2018). XPS studies of nitrogen doping niobium used for accelerator applications. *Applied Surface Science, 439*, 1119–1126.